Available online at www.sciencedirect.com
SCIENCE DIRECT®
ELSEVIER
Journal of Sound and Vibration 278 (2004) 825–846
JOURNAL OF SOUND AND VIBRATION
www.elsevier.com/locate/jsvi

A model for the damping of torsional vibration in thin-walled tubes with constrained viscoelastic layers

S.A. Nayfeh*, K.K. Varanasi

Department of Mechanical Engineering, Massachusetts Institute of Technology, Cambridge, MA 02139, USA

Received 25 October 2001; accepted 16 October 2003

Abstract

A model for torsional vibration of slender thin-walled tubes with constrained-layer dampers is developed. Assuming that the deformation obeys the Saint-Venant hypotheses, we develop a model suitable for prediction of the complex stiffness per unit length in closed, thin-walled tubes whose walls consist of laminated elastic and viscoelastic layers, and formulate a boundary-value problem for the warping deformations arising under Saint-Venant torsion. For some basic cross-sectional shapes, we solve the warping problem and thence obtain closed-form expressions for the complex stiffness per unit length. Next, we provide some guidelines for the design of tubes with high damping in torsion. Finally, we compare the damping predicted by the model to measurements performed on a simple structure.

1. Introduction

Consider the response of an elastic–viscoelastic beam to a harmonically varying twisting moment applied at its end. If the frequency of motion is low enough that the rotary inertia of the beam can be neglected, the internal twisting moment does not vary from section to section, and hence the strains developed in the beam are independent of the lengthwise co-ordinate. A slender beam therefore takes on a constant angle of twist per unit length, and cross-sections distant from either end of the beam rotate about the longitudinal axis without distortion in their own plane. But such rotation gives rise to shear stresses which, unless the cross-section is axially symmetric, cause it to warp in the longitudinal direction. This model for the torsion of slender beams was first proposed by Saint-Venant in 1855 and is referred to in the literature as ''uniform'' or ''Saint-Venant'' torsion.

*Corresponding author. Tel.: +1-617-253-2407; fax: +1-617-253-7549.
E-mail address: nayfeh@mit.edu (S.A. Nayfeh).

0022-460X/$ - see front matter
doi:10.1016/j.jsv.2003.10.055

Near the ends of the beam, the deformation may violate the premises of the Saint-Venant theory of torsion in two important ways:

1. Restraint against warping: if an end is restrained against warping—for example, by welding it to a solid block—the deformation will not be uniform near that end. This effect is well documented in the elasticity literature and is known in homogeneous beams to be most significant for sections with large flanges (e.g. [1,2]). It may also cause significant non-uniformity for elastic–viscoelastic beams because, as we will see subsequently, warping displacements play an essential role in damping torsional vibration.
2. In-plane distortion: depending on the distribution of stresses on the end of a beam, cross-sections near that end may deform in their own plane. For homogeneous beams, this deformation can almost always be neglected, but for elastic–viscoelastic beams we can envision cases where it is of primary importance. Consider for example a beam made up of a circular elastic core and concentric viscoelastic and elastic layers. Suppose we exert a moment at one end of this beam on only the outer elastic layer. Near this end, the outer layer will undergo a larger rotation than the circular core, and this difference in rotation induces large strains in the viscoelastic layer. This mechanism of damping was studied by Chandrasekharan and Ghosh [3] and Batra and Yu [4] for straight beams and Nandakishore and Ghosh [5] for coil springs. To the best of the authors' knowledge, these are the only published works on non-uniform torsion of elastic–viscoelastic beams.

It is difficult to form a general measure of the importance of warping restraints and in-plane distortion; their effects must be evaluated on a case-by-case basis taking detailed account of the boundary conditions. In the present study, we will work under the assumptions of Saint-Venant torsion.

Upon review of the literature we find only a handful of studies of Saint-Venant torsion of elastic–viscoelastic beams: Johnson and Woolf [6] examine torsion of a two-layer beam made up of a thick elastic bar and a thin viscoelastic layer. Starting from the classical formulation given by Sokolnikoff [7] for the stress distribution in a compound beam, they derive a perturbation solution valid when the viscoelastic layer is much more compliant than the elastic layer. From a similar formulation, Dewa [8] generates numerical solutions for three-layer elastic–viscoelastic beams made up of solid rectangular laminae. Other researchers have studied bending and torsion of laminated rectangular beams composed of anisotropic laminae (e.g. [9,10]).

Closed, thin-walled tubes have high flexural and torsional stiffnesses for a given mass, and therefore find wide application in machine and aerospace structures. Demoret [11] studied round tubes with slender constraining layers wrapped helically around their circumference in order to damp both torsional and bending vibration. In the present work, we develop a general model for torsion of closed, thin-walled, elastic–viscoelastic tubes with constrained viscoelastic layers that extend along the length of the tube. Assuming that the deformation obeys the Saint-Venant assumptions and neglecting the rotary inertia of the compound tube, we develop a boundary-value problem for the warping displacements of the tube wall. Next, for the specific cases of circular and rectangular tubes, we solve the warping problem and obtain expressions for the torsional complex stiffness per unit length.

Finally, we present measurements of the resonant frequencies and loss factors for torsional vibration of a square steel tube with constrained viscoelastic layers. The shear modulus and loss

factor of the viscoelastic material are varied by changing the temperature of the specimen while conducting a series of measurements. The measured values are in close agreement with those predicted by the model.

2. Modelling and analysis

Because we neglect rotary inertia in our analysis, harmonic motion is governed in the frequency domain by equations of the same form as those governing static deformation. We note, however, that the following derivations are carried out in the frequency domain and that the deformations, stresses, and strains are harmonically varying quantities whose magnitude and phase are represented by complex variables. Consider, as shown in Fig. 1, a closed elastic tube of modulus G_1 to which is attached a thin viscoelastic layer of modulus G_2 backed by an elastic constraining layer of modulus G_3. The thin-walled tube forms a single closed loop in the yz plane, and its shape is given by the vector $\mathbf{R}(s)$ normalized so that $\mathrm{d}\mathbf{R}/\mathrm{d}s = \mathbf{e}_s$.

2.1. Modelling assumptions

According to the Saint-Venant model, imposition of a twisting moment develops shear stresses in the yz plane. In the absence of laminated viscoelastic layers these stresses run parallel to the tube wall, and the shear flow $t\tau_{xs}$ is constant. In the present case, the shear flow $t_1(\tau_{xs})_1$ is constant only on that portion of the tube wall without lamination. On the laminated region, some stress is transmitted through the viscoelastic layer to the constraining layer, and the total shear flow $t_1(\tau_{xs})_1 + t_2(\tau_{xs})_2 + t_3(\tau_{xs})_3$ must be constant.

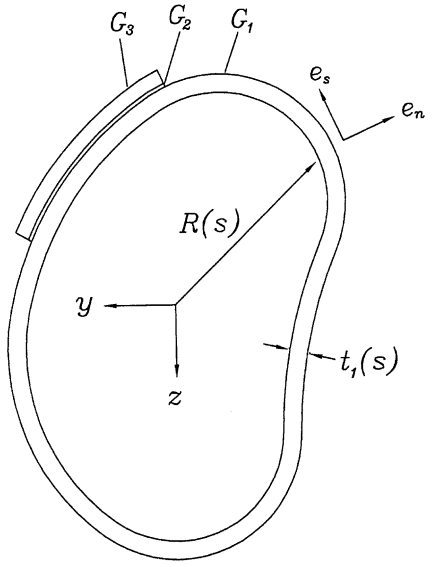

Fig. 1. Cross-section of a thin-walled tube consisting of a closed elastic tube of modulus G_1 and thickness $t_1(s)$, a viscoelastic layer of (complex) modulus G_2 and thickness $t_2(s)$, and a constraining layer of modulus G_3 and thickness $t_3(s)$.

It follows immediately from the Saint-Venant assumptions that the only non-zero stresses are the shear stresses τ_{xs} in the tangential direction and τ_{xn} in the normal direction. So the differential equation of equilibrium in the ith layer is given by

$$\frac{\partial(\tau_{xn})_i}{\partial n} + \frac{\partial(\tau_{xs})_i}{\partial s} = 0. \tag{1}$$

Rather than attack this equation directly, we introduce the following modelling assumptions:

1. The viscoelastic material is far more compliant than the elastic layers and can be modelled as a frequency-independent hysteretic material with a complex stiffness (e.g. [12]).
2. At the interface between a viscoelastic layer and an elastic layer, the displacements in the tangential direction—and hence the shear strains in the tangential direction—must match. We therefore take the shear strain $(\gamma_{xs})_2$ in the viscoelastic layers to be of the same order as the shear strains $(\gamma_{xs})_1$ and $(\gamma_{xs})_3$ in the adjoining elastic layers. But the viscoelastic layer is far more compliant than either of the elastic layers, and therefore the shear stress $(\tau_{xs})_2$ in the tangential direction in the viscoelastic layer is negligible in comparison to $(\tau_{xs})_1$ and $(\tau_{xs})_3$ in the elastic layers.
3. The shear stress $(\tau_{xn})_2$ in the normal direction in the viscoelastic layer is of the same order as $(\tau_{xn})_1$ and $(\tau_{xn})_3$ in the elastic layers, but the viscoelastic layer is far more compliant. Hence the shear strains $(\gamma_{xn})_1$ and $(\gamma_{xn})_3$ in the elastic layers can be neglected in comparison to $(\gamma_{xn})_2$ in the viscoelastic layer.
4. The shear stresses in the normal direction must vanish at the inner and outer walls of the tube, so it follows from Eq. (1) that, in the first elastic layer, $(\tau_{xn})_1 \sim (\tau_{xs})_1 t_1/R_0$, where R_0 is a characteristic length in the tangential direction and t_1 is the thickness of the inner elastic layer. Thus, for a thin-walled tube, we have $(\tau_{xn})_1 \ll (\tau_{xs})_1$. Likewise, in the constraining layer we have $(\tau_{xn})_3 \ll (\tau_{xs})_3$.
5. In the viscoelastic layer, the shear stress $(\tau_{xn})_2$ in the normal direction is of the same order as $(\tau_{xn})_1$ and $(\tau_{xn})_3$ in the elastic layers and hence (from item 3 above) is much smaller than $(\tau_{xs})_1$ or $(\tau_{xs})_3$.
6. The variation of $(\gamma_{xn})_2$ through the thickness of the viscoelastic layer and the variation of $(\tau_{xs})_1$ and $(\tau_{xs})_3$ through the thickness of the elastic layers can be neglected.

Summary: The shear *stress* in the direction tangent to the tube wall can be neglected in the viscoelastic layer but not in the elastic layers. Conversely, the shear *strain* in the direction normal to the tube wall can be neglected in the elastic layers but not in the viscoelastic layer. The shear stress in the tangential direction in the elastic layers and the shear strain in the normal direction in the viscoelastic layer can be treated as constants across the thickness of each layer. Moreover, the shear stresses are much larger in the tangential than in the normal direction.

2.2. Formulation

Consider a tube subject to an angle of twist per unit length of magnitude θ. Because the shear strains in the normal direction are negligible in the elastic layers, the warping displacements, u_1 in the tube wall and u_3 in the constraining layer, are functions of only the tangential co-ordinate s.

Therefore, making use of the Saint-Venant assumptions, the displacement of a point on the tube wall can be written as

$$(\Delta\mathbf{R})_i = u_i(s)\mathbf{e}_x + \theta x\mathbf{e}_x \times \mathbf{R}(s), \tag{2}$$

where x is the lengthwise co-ordinate and $\mathbf{e}_x$ is the unit vector pointing along the axis of the tube.

As was argued in the foregoing, a twisting moment is resisted primarily by shear stresses in the tangential direction in the elastic layers. Making use of the deformation given in Eq. (2), we can write the corresponding shear strain in the tube wall as

$$(\gamma_{xs})_1 = \frac{\mathrm{d}u_1}{\mathrm{d}s} + \frac{\mathrm{d}}{\mathrm{d}x}[(\Delta\mathbf{R})_1 \cdot \mathbf{e}_s] = \frac{\mathrm{d}u_1}{\mathrm{d}s} + \theta\mathbf{R} \cdot \mathbf{e}_n \tag{3}$$

and, likewise, in the constraining layer,

$$(\gamma_{xs})_3 = \frac{\mathrm{d}u_3}{\mathrm{d}s} + \frac{\mathrm{d}}{\mathrm{d}x}[(\Delta\mathbf{R})_3 \cdot \mathbf{e}_s] = \frac{\mathrm{d}u_3}{\mathrm{d}s} + \theta\mathbf{R} \cdot \mathbf{e}_n. \tag{4}$$

In the viscoelastic layer, we are concerned with the shear strain in the normal direction; assuming it is constant through the thickness of the viscoelastic layer, we write it in terms of the warping displacements as

$$(\gamma_{xn})_2 = \frac{u_3 - u_1}{t_2}, \tag{5}$$

where t_2 is the thickness of the viscoelastic layer.

In formulating the conditions for equilibrium, we examine first those portions of the tube wall not covered by a constrained viscoelastic layer. Consider a slice ds of this homogeneous wall. We have already argued that the only significant stress acting upon it is the shear stress in the direction tangent to the wall, and that this stress can be taken to be uniform through the thickness of the wall. Denoting this stress by $(\hat{\tau}_{xs})_1$ and summing forces in the x direction, we write the equation of equilibrium

$$\frac{\mathrm{d}}{\mathrm{d}s}[t_1(\hat{\tau}_{xs})_1] = 0 \tag{6}$$

from which we see that the shear flow $t_1(\hat{\tau}_{xs})_1$ is constant on homogeneous segments of the tube wall.

On portions of the tube wall covered by a constrained viscoelastic layer, we must also consider the resultant of the normal stress transmitted through the viscoelastic layer. Hence, the force balance of the tube wall is of the form

$$\frac{\mathrm{d}}{\mathrm{d}s}[t_1(\tau_{xs})_1] + (\tau_{xn})_2 = 0. \tag{7}$$

Similarly, for the constraining layer we have

$$\frac{\mathrm{d}}{\mathrm{d}s}[t_3(\tau_{xs})_3] - (\tau_{xn})_2 = 0. \tag{8}$$

If we combine Eqs. (7) and (8), we see that the total shear flow $t_1(\tau_{xs})_1 + t_3(\tau_{xs})_3$ is constant on laminated segments of the tube wall. (Recall that $t_2(\tau_{xs})_2$ is negligible.)

Now introducing the shear moduli G_1, G_2, and G_3 for the tube wall, viscoelastic, and constraining layers, respectively, we can use the shear strains given in Eqs. (3)–(5) to write the equations of equilibrium (6)–(8) in terms of the warping displacements. On homogeneous segments of the wall, we obtain

$$\frac{\mathrm{d}}{\mathrm{d}s}\left[G_1 t_1\left(\frac{\mathrm{d}\hat{u}_1}{\mathrm{d}s} + \theta\mathbf{R}\cdot\mathbf{e}_n\right)\right] = 0, \tag{9}$$

where we have introduced the notation $\hat{u}_1$ for the warping displacement on a homogeneous segment of the wall. On laminated segments of the wall, we obtain

$$\frac{\mathrm{d}}{\mathrm{d}s}\left[G_1 t_1\left(\frac{\mathrm{d}u_1}{\mathrm{d}s} + \theta\mathbf{R}\cdot\mathbf{e}_n\right)\right] + \frac{G_2}{t_2}(u_3 - u_1) = 0 \tag{10}$$

for the tube wall and

$$\frac{\mathrm{d}}{\mathrm{d}s}\left[G_3 t_3\left(\frac{\mathrm{d}u_3}{\mathrm{d}s} + \theta\mathbf{R}\cdot\mathbf{e}_n\right)\right] - \frac{G_2}{t_2}(u_3 - u_1) = 0 \tag{11}$$

for the constraining layer.

The warping displacements are governed by Eq. (9) on homogeneous regions of the tube wall and by Eqs. (10) and (11) on laminated regions of the tube wall. Our task is to solve these equations subject to the following conditions:

1. The shear stress $(\tau_{xs})_3$ must vanish at the ends of a constraining layer. In terms of the warping displacement, this condition takes the form
$$\frac{\mathrm{d}u_3}{\mathrm{d}s} + \theta\mathbf{R}\cdot\mathbf{e}_n = 0. \tag{12}$$

2. At junctions between laminated and homogeneous segments of the wall, the stresses in the tangential direction as well as the warping displacements must match; that is, $u_1 = \hat{u}_1$ and $(\tau_{xs})_1 = (\hat{\tau}_{xs})_1$ at the ends of a constraining layer.
3. The total moment is obtained by integrating the shear flow over the periphery of the section, and since the total shear flow is constant, we can evaluate it on a homogeneous segment of the wall where it is given by $t_1(\hat{\tau}_{xs})_1$. Integrating around the perimeter of the section, we obtain
$$M_t = \oint (t_1(\hat{\tau}_{xs})_1)\mathbf{R}\cdot\mathbf{e}_n\,\mathrm{d}s = 2A[t_1(\hat{\tau}_{xs})_1], \tag{13}$$
which, when combined with Eq. (3), yields
$$M_t = 2A\left[G_1 t_1\left(\frac{\mathrm{d}\hat{u}_1}{\mathrm{d}s} + \theta\mathbf{R}\cdot\mathbf{e}_n\right)\right], \tag{14}$$

where A is the area enclosed by the tube wall. The quantity in brackets can be evaluated anywhere on the homogeneous segments of the wall.

In the following sections, we use this formulation to derive expressions for the complex stiffness for some specific cross-sections. We begin by considering a round tube with a single laminated viscoelastic segment, and then generalize the results to round tubes with multiple symmetric laminated regions. Finally, we obtain solutions for rectangular tubes with all four faces laminated.

2.3. Circular tube with a constrained viscoelastic layer

Consider the cross-section shown in Fig. 2, which consists of a circular tube of radius r and constant wall thickness t_1 to which is laminated a viscoelastic layer of thickness t_2 backed by a constraining layer of thickness t_3.

We set the origin of the tangential co-ordinate system at the center of the constraining layer so that the ends of the constraining layer are at $s = \pm a$. We also find it convenient to develop solutions in terms of the parameter b, which at present we set equal to πr so that $s = \pm b$ is the location on the tube wall directly opposite the midpoint of the constrained viscoelastic layer.

2.3.1. Warping displacements

For a circular tube with constant wall thickness, Eqs. (10) and (11) governing the warping displacements u_1 and u_3 on laminated regions of the tube reduce to

$$G_1 t_1 \frac{\mathrm{d}^2 u_1}{\mathrm{d}s^2} + \frac{G_2}{t_2}(u_3 - u_1) = 0, \tag{15}$$

$$G_3 t_3 \frac{\mathrm{d}^2 u_3}{\mathrm{d}s^2} - \frac{G_2}{t_2}(u_3 - u_1) = 0. \tag{16}$$

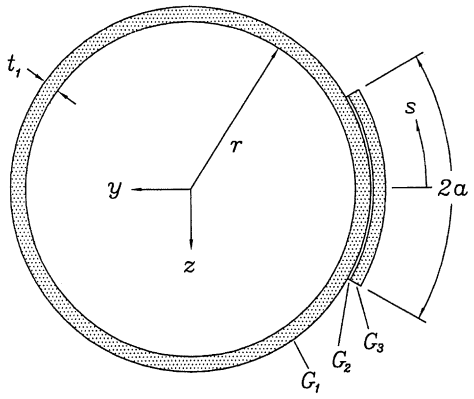

Fig. 2. Cross-section of a circular tube with a single constrained viscoelastic layer: the tube wall has shear modulus G_1, thickness t_1, and perimeter $2b$. The constrained viscoelastic layer extends over a length $2a$ of the tube wall and consists of a viscoelastic layer with complex modulus G_2 and thickness t_2 backed by an elastic layer with modulus G_3 and thickness t_3.

The general solution of this system of homogeneous equations can be written in the form

$$\begin{bmatrix} u_1 \\ u_3 \end{bmatrix} = (c_1 + c_2 s)\begin{bmatrix} 1 \\ 1 \end{bmatrix} + \left(c_3 \sinh\frac{g_t s}{a} + c_4 \cosh\frac{g_t s}{a}\right)\begin{bmatrix} 1 \\ \kappa \end{bmatrix}, \tag{17}$$

where $\kappa = -G_1 t_1/G_3 t_3$, the c_i are constants to be determined from the matching conditions, and the eigenvalue g_t/a is given by

$$\frac{g_t}{a} = \sqrt{\frac{G_2}{t_2}\left(\frac{G_1 t_1 + G_3 t_3}{G_1 t_1 G_3 t_3}\right)\left(\frac{a}{b}\right)} = \sqrt{\frac{G_2}{t_2}\left(\frac{1}{G_1 t_1 Y}\right)\left(\frac{a}{b}\right)}, \tag{18}$$

where

$$Y = \frac{G_3 t_3}{G_1 t_1 + G_3 t_3}\left(\frac{a}{b}\right). \tag{19}$$

Examining the form of g_t/a given above, we see that it is a measure of the stiffness of the viscoelastic layer relative to that of the elastic layers. It plays a role similar to the so-called coupling parameter that characterizes constrained-layer damping of bending vibration (e.g. [13]). Similarly, if k_0 is the torsional stiffness of the tube without constraining layers and k_∞ is the torsional stiffness of the tube with the constraining layers rigidly attached, the dimensionless parameter Y can be written as

$$Y = \frac{k_\infty - k_0}{k_\infty}. \tag{20}$$

It plays the same role as the so-called stiffness or geometric parameter in bending vibration. As we shall see, the dimensionless parameters g_t and Y fully determine the complex stiffness of the composite tube.

On regions of the tube without lamination, the warping displacement $\hat{u}_1$ is governed by Eq. (9), which for a circular tube with constant wall thickness reduces to

$$G_1 t_1 \frac{\mathrm{d}^2 \hat{u}_1}{\mathrm{d}s^2} = 0, \tag{21}$$

whose general solution we write in the form

$$\hat{u}_1 = c_5 s + c_6, \tag{22}$$

where c_5 and c_6 are constants. Whereas an axially symmetric tube does not warp, we see from the warping displacements given by Eqs. (22) and (17) that the addition of the constrained viscoelastic layer causes the tube wall to warp and to take on some curvature on regions with lamination.

We are not concerned here with rigid-body motions of the tube, and hence set them to zero and make use of symmetry arguments to conveniently determine the constants c_1 to c_6. The warping displacements go to zero on the axis of symmetry; thus, at $s = 0$ we have

$$u_1(0) = u_3(0) = 0 \tag{23}$$

and at $s = b = \pi r$ we have

$$\hat{u}_1(b) = 0. \tag{24}$$

At $s = a$, the shear stress in the constraining layer must vanish. This condition, set forth in Eq. (12), reduces to

$$\frac{\mathrm{d}u_3(a)}{\mathrm{d}s} + r\theta = 0 \tag{25}$$

for a circular tube. In the tube wall, the displacements must match:

$$u_1(a) = \hat{u}_1(a). \tag{26}$$

The shear stresses must also match. Using Eq. (3), we write

$$\frac{\mathrm{d}u_1(a)}{\mathrm{d}s} = \frac{\mathrm{d}\hat{u}_1(a)}{\mathrm{d}s}. \tag{27}$$

The six matching conditions given in Eqs. (23)–(27) determine the constants c_1 through c_6 in terms of the angle of twist per unit length θ.

Substituting the warping displacements (22) and (17) into the matching conditions (23)–(27), and solving for the c_i, we write the warping displacements in the form

$$\hat{u}_1 = \frac{br\theta Y\lambda}{1-\lambda Y}\left(\frac{s}{b} - 1\right) \tag{28}$$

and

$$\begin{bmatrix} u_1 \\ u_3 \end{bmatrix} = \frac{br\theta Y}{1 - Y\lambda}\left\{\frac{\sinh g_t s/a}{g_t \cosh g_t}\begin{bmatrix} 1 \\ \kappa \end{bmatrix} + \left(\lambda - \frac{b}{a}\right)\left(\frac{s}{b}\right)\begin{bmatrix} 1 \\ 1 \end{bmatrix}\right\}, \tag{29}$$

where g_t is defined in Eq. (18), Y is defined in Eq. (19), and

$$\lambda = 1 - \frac{\tanh g_t}{g_t}. \tag{30}$$

We can now plot the warping displacements as shown in Fig. 3, where we illustrate the effect of increasing g_t for fixed Y and a/b. For small g_t, the tube wall and the constraining layer are nearly decoupled: the tube wall warps only slightly and the constraining layer suffers little shear deformation as it undergoes a large rigid-body rotation. As g_t is increased, the coupling becomes stronger, and we see that for large g_t the tube wall is strongly warped. We expect that the damping will be highest at intermediate values of g_t where the coupling is strong enough to induce significant stress into the constraining layer, but weak enough to allow significant strain.

2.3.2. Complex stiffness

Substituting the expression for $\hat{u}_1$ given by Eq. (28) into the integral condition for the total moment on the tube set forth in Eq. (14), we obtain

$$k_t(1 + \mathrm{j}\eta_t \operatorname{sgn}\omega) = \frac{M_t}{\theta}\left(\frac{P}{4A^2 G_1 t_1}\right) = \frac{1}{1-\lambda Y}, \tag{31}$$

where k_t is the normalized static stiffness of the tube and η_t is its loss factor. It is necessary to multiply the loss factor η_t by $\operatorname{sgn}\omega = \omega/|\omega|$ to avoid fallacious results in the inverse Fourier transform [12,14]. The parameter Y, as we have seen, depends only on the material properties and dimensions of the tube wall and constraining layer, whereas λ is a function of g_t, which is a measure of the stiffness of the viscoelastic layer. Modelling the viscoelastic material as

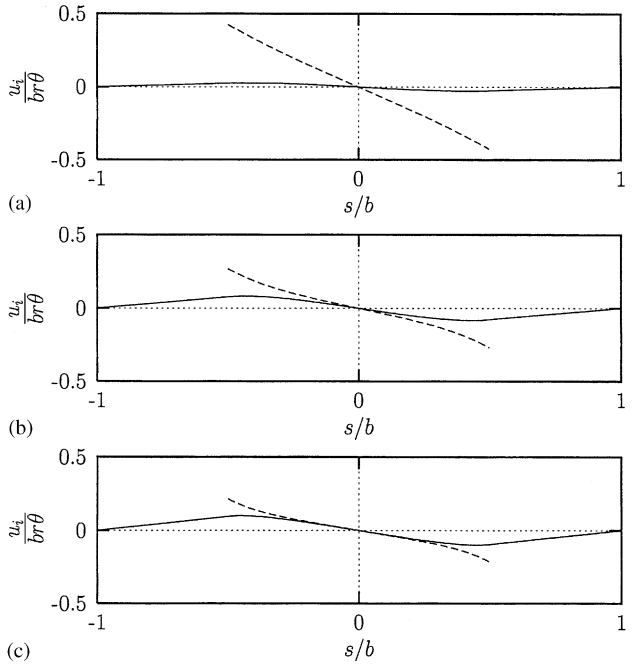

Fig. 3. Static normalized warping displacements $u_1/br\theta$ (solid line) and $u_3/br\theta$ (dashed line) in a circular tube with a single constrained viscoelastic layer; $a/b = 0.5$, $Y = 0.2$, $\kappa = 1.5$, and (a) $g_t = 1$, (b) $g_t = 3$, and (c) $g_t = 5$.

frequency-independent hysteretic, we write its complex shear modulus as $G_2 = G_v(1 + j\eta_v \operatorname{sgn}\omega)$ and rewrite Eq. (18) as

$$g_t = \sqrt{(1 + j\eta_v \operatorname{sgn}\omega)\frac{a^2 G_v}{t_2}\left(\frac{1}{G_1 t_1 Y}\right)\left(\frac{a}{b}\right)}. \tag{32}$$

The dependence of λ on g_t is given in Eq. (30), from which we see that λ approaches zero for small $|g_t|$ and unity for large $|g_t|$. At intermediate magnitudes of complex g_t, λ takes on complex values, yielding non-zero η_t.

In Fig. 4, we have fixed $\eta_v = 1$ and plotted the stiffness and loss factor as a function of the real part of g_t. As expected, the damping is maximized at intermediate magnitudes of g_t. Since Y and λ appear as products in Eq. (31) for the torsional stiffness, the damping potential can be improved by increasing Y.

2.4. Circular tube with multiple constrained viscoelastic layers

In this section, we consider torsion of a thin-walled tube with multiple constrained viscoelastic layers arranged symmetrically on the tube wall. As shown in Fig. 5, each of the N identical constrained viscoelastic layers extends over a length $2a$ of the tube wall of total perimeter $2Nb$.

The equations of equilibrium take on exactly the same form as they did for a tube with a single constraining layer of length $2a$ on a tube of perimeter $2b$, so Eqs. (15), (16), and (21) governing the

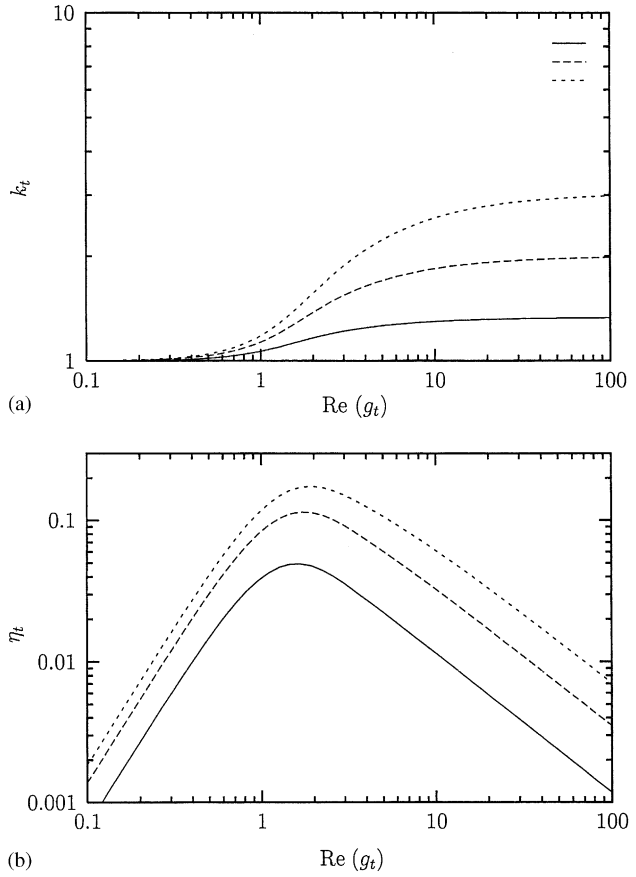

Fig. 4. (a) Static stiffness and (b) loss factor, plotted against the real part of g_t for a circular tube with a single constrained viscoelastic layer with $\eta_v = 1$ and $Y = 0.25$ (solid), 0.50 (long dashes), and 0.67 (short dashes).

warping displacements are still valid for this case. The boundary conditions matching displacements and stresses at the ends of the constraining layers are unchanged, and we can again argue from symmetry that the warping displacements must vanish at $s = 0$ and integer multiples of b. So we can also reuse the boundary conditions given in Eqs. (23)–(27). Thus the solutions for the warping displacements on $-b \leqslant s \leqslant b$ are independent of the number of constrained viscoelastic layers arranged around the section, and the warping displacements on $-Nb \leqslant s \leqslant Nb$ can be constructed simply by stringing the displacements on $-b \leqslant s \leqslant b$ together as shown in Fig. 6.

The torsional stiffness of a composite tube with multiple constrained viscoelastic layers can be derived by the same method used for a tube with a single constrained viscoelastic layer, and we find that the result given in Eq. (31) is unchanged. Thus, for identical values of Y and λ, the same complex torsional stiffness is obtained for any number of symmetrically arranged constrained viscoelastic layers.

This leads to some simple laws for scaling design parameters. Suppose for example that we have found a design using a single constrained viscoelastic layer which yields a favorable complex

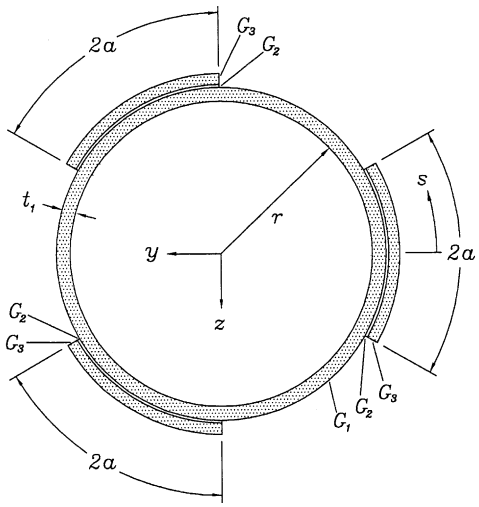

Fig. 5. Cross-section of a circular tube with three constrained viscoelastic layers arranged symmetrically on its perimeter: the tube wall has modulus G_1, thickness t_1, and perimeter $6b$. Each of the constrained viscoelastic layers extends over a length $2a$ of the tube wall, and consists of a viscoelastic layer of complex modulus G_2 and thickness t_2 and elastic layer of modulus G_3 and thickness t_3.

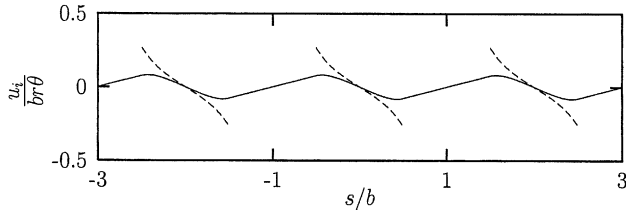

Fig. 6. Static normalized warping displacements $u_1/br\theta$ (solid line) and $u_3/br\theta$ (dashed line) in a circular tube with three constrained viscoelastic layers arranged symmetrically on the tube wall; $a/b = 0.5$, $Y = 0.2$, $\kappa = 1.5$, and $g_t = 3$.

stiffness but requires the use of an unreasonably thick viscoelastic layer. If we split the constraining layer into four segments and hold $a/b, t_1, t_3$, and the material properties constant, Y does not change. Then from Eq. (18), we see that to obtain the same value of g_t (and therefore the same value of λ) we must scale the thickness t_2 of the viscoelastic layer with a^2. Thus, in our example, by cutting the constraining layer into four segments, we can reduce the thickness of the viscoelastic layer by a factor of 16 without changing the complex stiffness.

2.5. Rectangular tubes

Consider the rectangular tube with constrained viscoelastic layers shown in Fig. 7. The faces of the tube that extend in the y direction have thickness t_1, shear modulus G_1, and length $2h$. These faces are covered completely by viscoelastic layers of thickness t_2 and shear modulus G_2, which in turn are covered by elastic layers of thickness t_3 and modulus G_3. The faces of the tube that extend

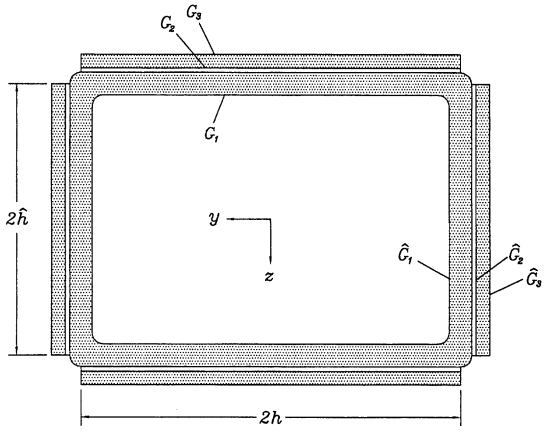

Fig. 7. Cross-section of a rectangular tube: The tube is symmetric about both the y- and z-axis.

in the z direction have a similar layup, but possibly different dimensions and material properties. These are denoted in the like manner, but with the addition of a hat (e.g., $\hat{t}_1$, $\hat{G}_1$).

2.5.1. Warping displacements

Examining Eqs. (10) and (11), we note that the quantity $\mathbf{R}\cdot\mathbf{e}_n$ is simply the normal distance from the origin to the face of the tube, and hence its derivative vanishes along any face of the tube. In the corners of the tube, the normal distance changes rapidly with s, but even large strains on such a localized region cannot lead to large warping deflections, and we can safely ignore the corner effects when solving for the overall warping deflections in the tube.

On the segment of the tube from $y=-h$ to h, Eqs. (10) and (11) governing the warping displacements $u_1(y)$ and $u_3(y)$ become

$$G_1 t_1 \frac{\mathrm{d}^2 u_1}{\mathrm{d}y^2} + \frac{G_2}{t_2}(u_3 - u_1) = 0 \tag{33}$$

and

$$G_3 t_3 \frac{\mathrm{d}^2 u_3}{\mathrm{d}y^2} - \frac{G_2}{t_2}(u_3 - u_1) = 0, \tag{34}$$

whose general solution we denote

$$\begin{bmatrix} u_1 \\ u_3 \end{bmatrix} = (c_1 + c_2 y)\begin{bmatrix} 1 \\ 1 \end{bmatrix} + \left(c_3 \sinh\frac{g_t y}{h} + c_4 \cosh\frac{g_t y}{h}\right)\begin{bmatrix} 1 \\ \kappa \end{bmatrix}, \tag{35}$$

where $\kappa = -G_1 t_1 / G_3 t_3$ and, in agreement with the results for a round tube with $a=b$ given in Eqs. (18) and (19),

$$g_t = \sqrt{\frac{G_2}{t_2}\left(\frac{h^2}{G_1 t_1 Y}\right)} \tag{36}$$

and

$$Y = \frac{G_3 t_3}{G_1 t_1 + G_3 t_3}. \tag{37}$$

On the segment from $z = -\hat{h}$ to $\hat{h}$, the warping displacements $\hat{u}_1(z)$ and $\hat{u}_3(z)$ are governed by

$$\hat{G}_1 \hat{t}_1 \frac{\mathrm{d}^2 \hat{u}_1}{\mathrm{d}z^2} + \frac{\hat{G}_2}{\hat{t}_2}(\hat{u}_3 - \hat{u}_1) = 0, \tag{38}$$

$$\hat{G}_3 \hat{t}_3 \frac{\mathrm{d}^2 \hat{u}_3}{\mathrm{d}z^2} - \frac{\hat{G}_2}{\hat{t}_2}(\hat{u}_3 - \hat{u}_1) = 0, \tag{39}$$

whose solution we write as

$$\begin{bmatrix} \hat{u}_1 \\ \hat{u}_3 \end{bmatrix} = (c_5 + c_6 z)\begin{bmatrix} 1 \\ 1 \end{bmatrix} + \left(c_7 \sinh \frac{\hat{g}_t z}{\hat{h}} + c_8 \cosh \frac{\hat{g}_t z}{\hat{h}} \right) \begin{bmatrix} 1 \\ \hat{\kappa} \end{bmatrix}, \tag{40}$$

where $\hat{\kappa} = -\hat{G}_1 \hat{t}_1 / \hat{G}_3 \hat{t}_3$, and $\hat{g}_t$ and $\hat{Y}$ are defined as in Eqs. (36) and (37) but with the addition of hats on all quantities. The constants c_1 through c_8 are determined by the imposition of eight matching conditions.

The cross-section of the tube has two axes of symmetry, so the warping displacements must vanish at the midpoints of the walls:

$$u_1(0) = u_3(0) = 0, \tag{41}$$

$$\hat{u}_1(0) = \hat{u}_3(0) = 0. \tag{42}$$

Because of the symmetry, we can restrict our attention to the upper left quadrant of the cross-section in Fig. 7, and we need to establish matching conditions at only one corner. The displacement and shear flow in the tube walls must match at a corner. Hence, at $y = h$ and $z = \hat{h}$, we write

$$u_1(h) = \hat{u}_1(\hat{h}) \tag{43}$$

and

$$G_1 t_1 \left(\frac{\mathrm{d}u_1(h)}{\mathrm{d}y} + \theta \hat{h} \right) = \hat{G}_1 \hat{t}_1 \left(-\frac{\mathrm{d}\hat{u}_1(\hat{h})}{\mathrm{d}z} + \theta h \right), \tag{44}$$

where we have made use of the expression for shear strain given in Eq. (3). At the ends of the constraining layers, the shear stresses must go to zero; in terms of the displacements, this condition takes the form

$$\frac{\mathrm{d}u_3(h)}{\mathrm{d}y} + \theta \hat{h} = 0, \tag{45}$$

$$-\frac{\mathrm{d}\hat{u}_3(\hat{h})}{\mathrm{d}z} + \theta h = 0. \tag{46}$$

Now using the eight matching conditions (41)–(46) to solve for the c_i, we can write the warping displacements $u_1(y)$ and $u_3(y)$ in the form

$$\begin{bmatrix} u_1 \\ u_3 \end{bmatrix} = \frac{2h\hat{h}\theta\sigma Y}{\Lambda}\left\{\frac{\sinh g_t y/h}{g_t \cosh g_t}\begin{bmatrix} 1 \\ \kappa \end{bmatrix} - \left(\kappa + \frac{\Lambda}{2\sigma Y}\right)\begin{bmatrix} 1 \\ 1 \end{bmatrix}\left(\frac{y}{h}\right)\right\}, \tag{47}$$

where

$$\Lambda = \sigma(1 - \lambda Y) + \hat{\sigma}(1 - \hat{\lambda}\hat{Y}) \tag{48}$$

and, as in the case of circular tubes,

$$\lambda = 1 - \frac{\tanh g_t}{g_t} \quad \text{and} \quad \hat{\lambda} = 1 - \frac{\tanh \hat{g}_t}{\hat{g}_t}. \tag{49}$$

The quantities σ and $\hat{\sigma}$ represent the shear compliances per unit length of the tube wall

$$\sigma = \frac{4h}{G_1 t_1} \quad \text{and} \quad \hat{\sigma} = \frac{4\hat{h}}{\hat{G}_1 \hat{t}_1}, \tag{50}$$

which are defined so that the torsional stiffness of the tube without constraining layers is $4A^2/(\sigma + \hat{\sigma})$. The warping displacements $\hat{u}_1(z)$ and $\hat{u}_3(z)$ take the same form as given in Eq. (47), but with y replaced by $-z$ and the hatted and unhatted quantities interchanged.

2.5.2. Torsional stiffness

The resultant moment is given by integrating the shear flow around the periphery. The total shear flow is constant and most easily evaluated near a corner, where the stress in the constraining layer is zero and the shear flow is concentrated in the tube wall. Therefore, we rewrite Eq. (14) for this case as

$$M_t = 2AG_1 t_1\left[\frac{\mathrm{d}u_1(h)}{\mathrm{d}y} + \theta\hat{h}\right], \tag{51}$$

which, upon substitution for u_1 from Eq. (47) yields

$$k_t(1 + \mathrm{j}\eta_t \operatorname{sgn}\omega) = \frac{M_t}{\theta}\left(\frac{\sigma + \hat{\sigma}}{4A^2}\right) = \frac{\sigma + \hat{\sigma}}{\sigma(1 - \lambda Y) + \hat{\sigma}(1 - \hat{\lambda}\hat{Y})}, \tag{52}$$

where η_t is the loss factor of the compound tube and k_t is the ratio of its static stiffness to that of the tube in the absence of constrained viscoelastic layers.

Comparing the form of the complex stiffness given in Eq. (52) to that in Eq. (31) for a circular tube, we see that damping treatments on round and rectangular tubes have essentially the same character, the only difference being a lower degree of symmetry in rectangular tubes. Suppose the tube is a square with constant wall thickness, so that $\sigma = \hat{\sigma}$. If we restrict our attention to damping treatments where the constrained viscoelastic layers mounted to each of the four faces of the tube are identical, we also have $Y = \hat{Y}$ and $\lambda = \hat{\lambda}$ and the normalized torsional stiffness given in Eq. (52) becomes

$$k_t(1 + \mathrm{j}\eta_t \operatorname{sgn}\omega) = \frac{1}{1 - Y\lambda}, \tag{53}$$

in full agreement with Eq. (31) for a fully covered circular tube. If instead we wish to mount dampers to only two faces of the tube, then we can set $\hat{\lambda}$ to zero and obtain

$$k_t(1 + j\eta_t \operatorname{sgn} \omega) = \frac{1}{1 - Y\lambda/2}, \tag{54}$$

which is in agreement with Eq. (31) for a circular tube with viscoelastic layers on half of its circumference.

3. Experiment

In this section, we report on experiments conducted on an "I" structure formed by welding square steel tubes as sketched in Fig. 8. The first torsional mode of vibration of this structure involves pure torsion of the middle beam and nearly rigid rotation of the end beams. To minimize damping at the joints, the welds at each end of the tube are continuous through the thickness and along the perimeter of the tube wall.

To make the experiment—especially the measurement of damping—as repeatable as possible, we suspend the structure using surgical tubing to approximate free–free boundary conditions. Next, we use an impact hammer [15] to provide impulsive excitations to the suspended structure at the position shown in Fig. 8. The response is measured by a three-axis accelerometer [15] located close to the point of excitation and the force-to-acceleration transfer function is computed using a HP35670A dynamic signal analyzer over 10 averages. Next, we use standard modal-curve-fitting software such as Star Modal [16] to extract the values of natural frequency and loss factor of the first torsional mode of the structure from the measured force-to-acceleration frequency response curve. In all the experiments, the measurements of frequency and loss factor are found to be repeatable to within 0.25 Hz and 0.0005, respectively. Prior to application of the constrained viscoelastic layers, we thus measure the frequency and loss factor of the first torsional mode to be 186.3 Hz and 10^{-4}, respectively.

Next, we employ Bostik 7132 two-part adhesive [17] to bond a 0.38 mm thick layer of layer of EAR C-1002 material [18] followed by a 3.1 mm thick bar of steel to each face of the central tube to form constrained viscoelastic layers as shown in Fig. 9.

The stiffness and loss factor of the C-1002 are available from the manufacturer's data sheets [18] and in some references [14], but we have found that the effective complex stiffness of the

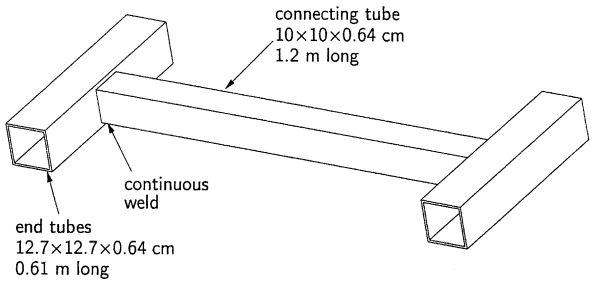

Fig. 8. Sketch of the welded steel frame used in the experiments.

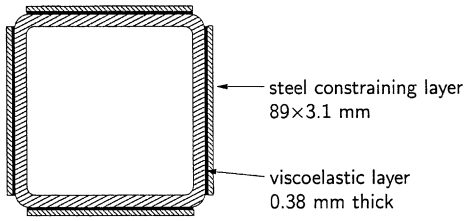

Fig. 9. Cross-section of the connecting tube with constrained viscoelastic layers.

Table 1
Material properties, predicted resonant frequency and damping, and measured resonant frequency and damping under varying temperature

Material properties			Predicted		Measured	
T (°C)	G_v (Mpa)	η_v	f (Hz)	η	f (Hz)	η
7.8	11.0	0.83	187.0	0.0248	189.5	0.0234
11.1	9.6	0.83	186.7	0.0222	189.0	0.0212
12.8	8.0	0.85	186.2	0.0196	188.5	0.0187
15.0	6.8	0.85	185.8	0.0171	188.2	0.0174
17.2	5.0	0.86	185.3	0.0132	187.4	0.0126
19.4	4.0	0.87	185.0	0.0109	187.1	0.0103
21.7	3.3	0.89	184.8	0.0093	186.8	0.0089
23.9	2.3	0.90	184.5	0.0067	186.3	0.0066

viscoelastic layer varies somewhat from lot to lot and with the adhesive used, so we detail in the Appendix a set of measurements in which we determine the complex shear stiffness of the viscoelastic material at various frequencies and temperatures. By interpolating among these measurements, we obtain the material properties shown in the first three columns of Table 1.

The structure is initially cooled to a temperature of approximately 7°C, and then brought slowly up to room temperature over the course of four hours. At each temperature shown in Table 1, we measure the force-to-acceleration frequency response, and then determine the natural frequencies and damping as described in the foregoing paragraphs. These results are reported in the last three columns of Table 1.

3.1. Theoretical predictions

As mentioned in the previous section, the first torsional mode of vibration of the test structure can be modelled as pure torsion of the middle beam and nearly rigid rotation of the end beams. Neglecting the inertia of the middle beam, we write the natural frequency f_n of the first torsional mode as

$$f_n = \frac{1}{2\pi}\sqrt{\frac{2\kappa_t}{J}}, \tag{55}$$

where κ_t is the torsional stiffness of the middle beam and J is the moment of inertia of the end beams. By substituting the value of the moment of inertia $J = 0.44$ kg m^2 for the end beams and the torsional stiffness $\kappa_t = 293$ kN m for the undamped middle beam (obtained using the well-known formula for the torsional stiffness of a thin-walled tube) in the above equation, we calculate the natural frequency f_n of the undamped structure as 183.8 Hz. We find that our prediction of the natural frequency is within 1.3% of the measured value.

Next we compute the natural frequencies and loss factors for the damped tube at various temperatures using the expression for the complex stiffness given in Eq. (52). In order to do so, we use Eq. (37) to determine that the stiffness parameter $Y \approx \frac{1}{3}$. For each value of the viscoelastic material properties, we obtain the shear parameter g_t from Eq. (36). The loss factor and normalized torsional stiffness per unit length are then computed from Eq. (52) and used to produce the results shown in Table 1. We find that the predicted results for the natural frequency and loss factor are within 1.2% and 8%, respectively, of the measured values. In Fig. 10, we compare the measured values of loss factor and stiffness to the theoretical results generated by holding the loss factor of the viscoelastic material at a constant value of 0.85. We find that the predicted results are in close agreement with the measured ones.

4. Discussion

We have seen that the complex stiffness of such a tube in torsion depends on two quantities for each constrained viscoelastic layer: one parameter of the generic form $Y = (k_\infty - k_0)/k_\infty$, which is a measure of the increase in stiffness that could be obtained by rigidly bonding the constraining layer to the tube wall, and a second parameter $g_t \propto (G_2/t_2)^{1/2}$ which is a measure of how strongly the viscoelastic layer couples the constraining layer to the tube wall. As in the case of constrained-layer damping of bending vibration, the highest damping is obtained by maximizing Y and holding g_t at an intermediate magnitude. For a given Y, the best value for g_t for a circular or square tube can be determined from Fig. 4. (For other geometries, use the theory given in Section 2.2.)

We often wish to design a damping treatment which damps both the torsional and bending vibration of a beam or a frame. Bending vibration of a thin-walled square tube of width $2h$ with constraining layers (of the same stiffness as the tube) mounted on all four faces is characterized by a geometric parameter $Y_b \approx 3t_3/4t_1$ and a shear parameter

$$g_b \approx \frac{G_2 \ell_e^2}{t_2 t_1 E_1} = \left(\frac{g_t \ell_e}{h}\right)^2 \left(\frac{G_1}{E_1}\right) \frac{t_3}{t_1 + t_3}, \tag{56}$$

where ℓ_e is the effective length of bending vibration (e.g. [19,20]). For the experiment discussed in this paper, we find that $\ell_e^2/h^2 \approx g_b/g_t^2$. The loss factor in bending will be optimized when g_b is between 0.1 and 1.0. But according to Fig. 4, the loss factor in torsion is highest when g_t is between unity and four. Thus it is difficult to obtain high damping in both torsion and bending if ℓ_e is much larger than h, as it would have to be for low-order modes of a slender beam. This suggests that segmenting the constraining layer (in order to make ℓ_e small) will allow us to optimize for both bending and torsion, but the model developed in this paper is not valid for torsion of such short constraining layers. Demoret [11] shows that slender constraining layers

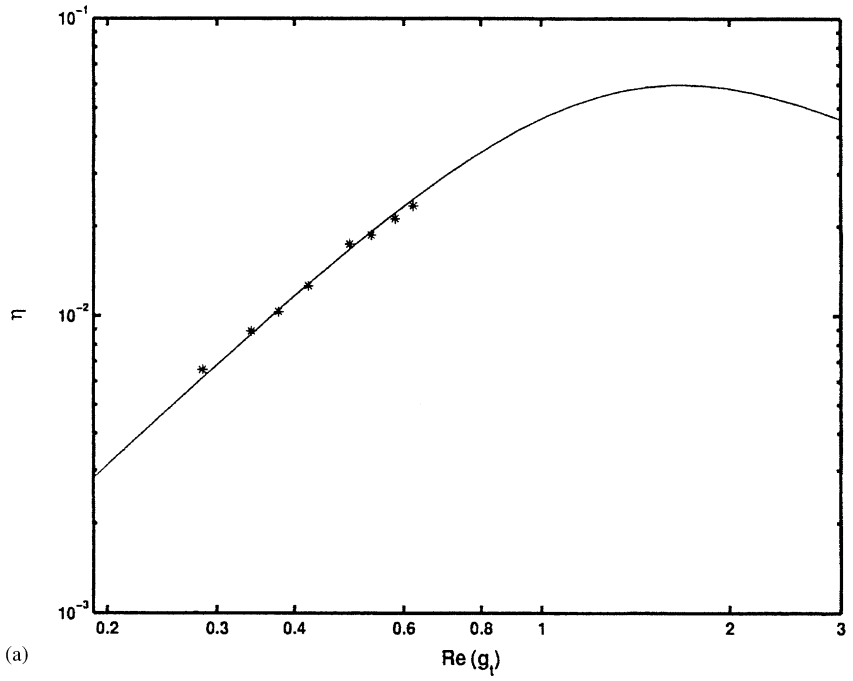

(a)

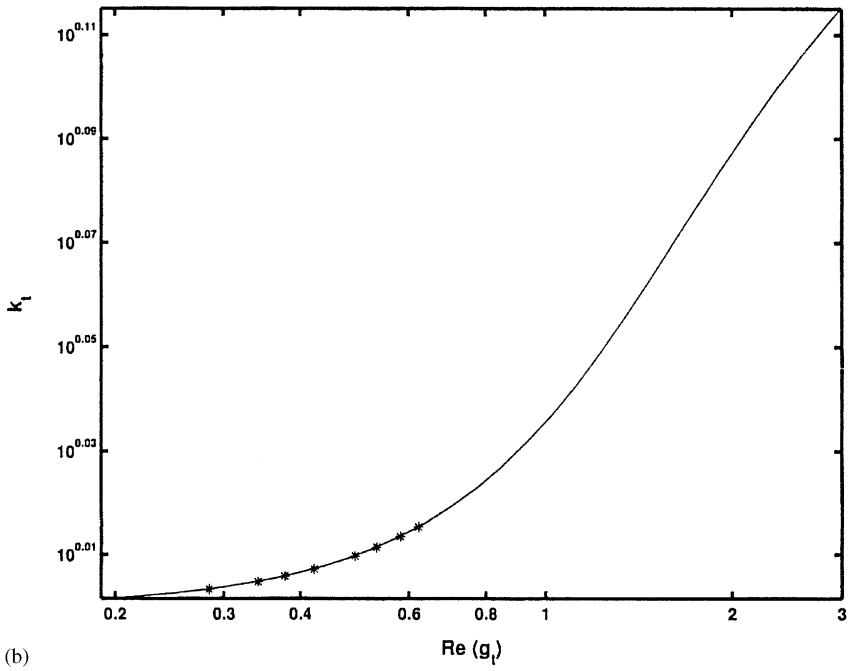

(b)

Fig. 10. Comparison of predicted and measured resonant frequency and loss factor for the experiment shown in Fig. 8.

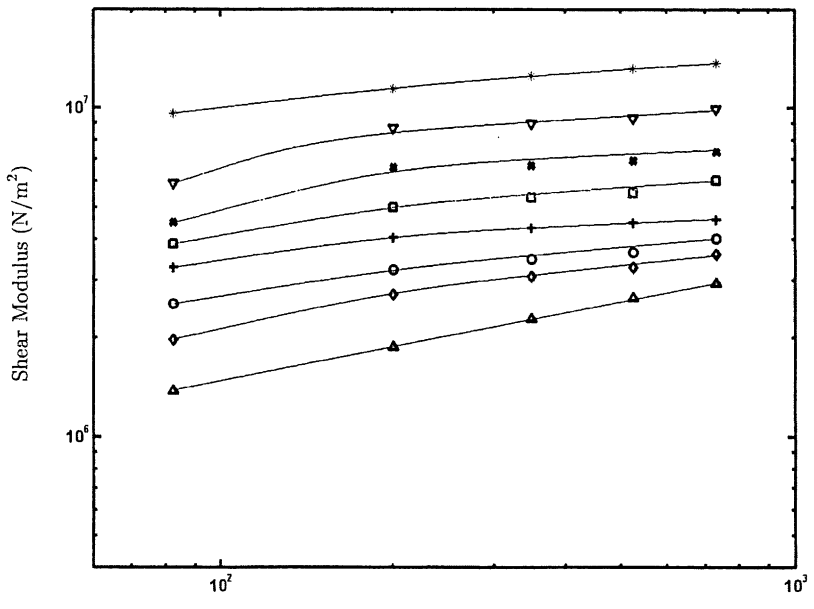

(a)

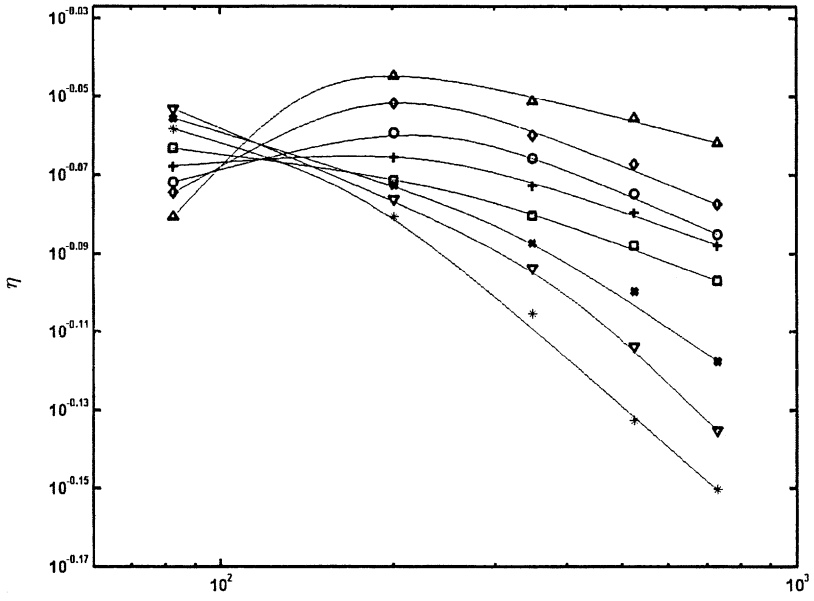

(b)

Fig. 11. (a) Shear modulus and (b) loss factor of the core material versus frequency at various temperatures: 7.8°C (∗), 12.2°C (∇), 14.4°C (×), 16.7°C (□), 18.9°C (+), 21.1°C (◦), 22.8°C (◇), 25.0°C (△).

wrapped helically around a circular tube can produce high damping in both torsion and bending. This has the effect of aligning the long dimension of the constraining layer with the principal stresses in the tube wall under torsion while aligning its short dimension with principal stresses in the tube wall under bending.

5. Conclusions and future work

In this paper, we have developed a model for uniform torsion of closed, thin-walled tubes with constrained viscoelastic layers and provided a framework for determination of their complex stiffness per unit length. We have found that the stress distribution and hence the complex stiffness in either case can be modelled with some fidelity in closed form, and therefore simple formulae can be used to optimize the damping of torsional vibration.

In our analysis, we have ignored the inertia effects and concentrated on determining the complex stiffness under uniform torsion. If one is faced with a problem with distributed loading or significant rotary inertia, the complex stiffness derived in this paper can be used to formulate a distributed-parameter model, provided that the characteristic length in the longitudinal direction is much larger than the cross-section.

We have restricted our attention to cross-sections where the wall-forms a single closed loop in the xy plane. But the modelling assumptions—and indeed, the equations governing the warping deflections—can be applied without modification to multi-cell tubes, though satisfying the matching conditions becomes somewhat more tedious.

In keeping with the classical Saint-Venant model of torsion, we have ignored all end effects, but because the structures we are concerned with in machine design are not always slender, it would be useful to develop some estimates of their importance. As we have seen, the warping deflections play a key role in damping the torsional vibration of elastic–viscoelastic beams, so restraining the ends of such beams from warping can have a major impact on their damping properties. It is also possible for an uneven stress distribution at the point of loading of an elastic–viscoelastic beam to cause its cross-section to deform within its own plane. To date, this effect has been studied only in beams with axially symmetric sections [3,4]. Moreover, as mentioned in Section 4, in many cases the design of a tube for high damping in both bending and torsion will require that the constraining layer be cut into relatively short segments. To design such dampers, the model presented in this paper must be modified to account for non-uniform torsion.

Appendix. Identification of the properties of the viscoelastic core

In this experiment, we measure the bending vibration of a symmetric sandwich beam in order to identify the properties of the viscoelastic core used in the torsional damping experiment described in Section 3. A three-layer sandwich beam consisting of aluminum elastic layers ($914 \times 51 \times 6.3\ \text{mm}^3$) and a layer of EAR C-1002 viscoelastic material (0.76 mm thick) was assembled using Bostik 7132 adhesive and suspended using light chords to approximate free–free boundary conditions. The shear modulus G_2 and loss factor η_2 of the viscoelastic material (at a frequency and temperature) were obtained from the resonant frequencies and loss factors of the first several

modes of the sandwich beam using results given by Nashif et al. [14]. The properties of the core material were thus obtained as functions of frequency and temperature and plotted in Fig. 11.

References

[1] S.P. Timoshenko, J.N. Goodier, *Theory of elasticity*, 3rd Edition, McGraw-Hill, New York, 1970.
[2] C.P. Kollbrunner, K. Basler, *Torsion in Structures*, Springer, New York, 1969.
[3] M.P. Chandrasekharan, A. Ghosh, Damping characteristics of elastic–viscoelastic composite shafts, *Journal of Sound and Vibration* 37 (1) (1974) 1–15.
[4] R.C. Batra, J.-H. Yu, Analysis of damping in finite shearing and torsional deformation, in: T.T. Hyde (Ed.), *Smart Structures and Materials: Damping and Isolation*, Newport Beach, CA, SPIE, Vol. 3969, 2000, pp. 86–98.
[5] N. Nandakishore, A. Ghosh, Damping characteristics of elastic–viscoelastic composite curved bars and helical springs, *Journal of Sound and Vibration* 43 (4) (1975) 621–632.
[6] A.F. Johnson, A. Woolf, Dynamic torsion of a two-layer viscoelastic beam, *Journal of Sound and Vibration* 48 (2) (1976) 251–263.
[7] I.S. Sokolnikoff, *Mathematical Theory of Elasticity*, McGraw-Hill, New York, 1956.
[8] H. Dewa, Torsional stress analysis and vibration damping of three-layered rods, *JSME International Journal* 33 (2) (1989) 152–159.
[9] T. Nouri-Baranger, P. Trompette, S. Shakhesi, Torsional vibrations of laminated beams: comparison of models, in: *Proceedings of the ASME Design Engineering Technical Conferences*, Vol. 7B, Las Vegas, NV, 1999, pp. 3113–3120.
[10] K.L. Napolitano, J.B. Kosmatka, Co-cured extension-twist coupled damped composite strut, *Journal of Composite Materials* 32 (21) (1998) 1914–1932.
[11] K.B. Demoret, The barberpole: constrained-layer damping for bending and torsion, in: C.D. Johnson (Ed.), *Passive Damping*, San Diego, CA, SPIE, Vol. 2445, 1995, pp. 350–361.
[12] S.H. Crandall, The hysteretic damping model in vibration theory, *Journal of Mechanical Engineering Science* 25 (1991) 23–28.
[13] D.J. Mead, *Passive Vibration Control*, Wiley, Sussex, 1999.
[14] A.D. Nashif, D.I.G. Jones, J.P. Henderson, *Vibration Damping*, Wiley, New York, 1985.
[15] Shock and Vibration Sensors Catalog, PCB Piezotronics, Depew, NY, 1999.
[16] The STAR System Reference Manual, Spectral Dynamics, Inc., San Jose, CA, 1998.
[17] Adhesive Data Sheet, Bostik Chemical Group, Middleton, MA, 1983.
[18] EAR Technical Data Sheet, E-A-R Speciality Composites, Indianapolis, IN.
[19] D.J. Mead, S. Markus, The forced vibration of a three-layer, damped sandwich beam with arbitrary boundary conditions, *Journal of Sound and Vibration* 10 (2) (1969) 163–175.
[20] S.A. Nayfeh, Design and Application of Damped Machine Elements, Ph.D. Thesis, Massachusetts Institute of Technology, Cambridge, MA, 1998.